Industrial Engineering Letters
ISSN 2224-6096 (Paper) ISSN 2225-0581 (online)
Vol.12, No.2, 2022

Computational Fluid Dynamic (CFD) Analysis of NACA Airfoil for Wind Turbine Blade Design

Ogbeide, O.O and Uwoghiren, F.O
Department of Production Engineering Faculty of Engineering, University of Benin, PMB 1154,
Benin City, Edo State, Nigeria
osarobo.ogbeide@uniben.edu; frank.uwoghiren@yahoo.com

Abstract
The paper presents a conceptual study of performance enhancing devices of an airfoil using computational Fluid Dynamics (CFD) technique. Two simple passive devices were selected and examined for increase in lift and decrease in drag. The target of the study was to evaluate and select the best airfoil suitable for wind turbine blade in a typical Nigeria Environment. The selected airfoils includes; NACA 0012, NACA 2412 and NACA 4412 while the selected angle of attack are; 0°, 4°, 8° and 12. The various airfoils geometry was created using Autodesk inventor and imported into ANSYS design modeler while meshing of the airfoil fluid geometry was done with the aid of ANSYS Meshing. To implement the ANSYS design modeller, the spalart-Allmaras turbulence model was selected and strain/vorticity based sub-option subsequently selected. The CAD Model was prepared in CATIA VS R19 while Pre-processing and simulation was done in ANSYS ICEM CFD 16.0 and ANSYS FLUENT 16.0 respectively. Result of the study shows that NACA 4412 at 4° angle of attack gave the maximum lift to drag ratio and hence, was considered for use in the design of wind turbine blade. The results justify the optimum position for enhancing airfoil performance at a specified angle of attack
Keywords: Airfoil, Wind turbine blade, Angle of attack, Coefficient of lift, Coefficient of drag and CFD analysis
DOI: 10.7176/IEL/12-2-03
Publication date: May 31st 2022

1. Introduction

Aerodynamics performance is fundamental for efficient rotor design (Maalawi and Badr, 2003).Aerodynamics lift is the force responsible for the power yield generated by the turbine and it is therefore essential to maximize this force using appropriate design. A resistant drag force which opposes the motion of the blade is also generated by friction which must be minimized. It is then apparent that an aerofoil section with a high lift to drag ratio typically greater than 30 be chosen for rotor blade design (Maalawi and Badr, 2003). The structural requirements of turbine blades signify that aerofoil with a high thickness to chord ratio be used in the root region. Thick aerofoil sections generally have a lower lift to drag ratio. Special consideration is therefore made for increasing the lift of thick aerofoil sections for use in wind turbine blade designs. (Rooij and Timmer, 2003; Fuglsang and Bak, 2004). Airfoil or aero foil is the aerodynamic cross section of a body such as a wing that creates lift as it moves through air or fluid. An airfoil-shaped body moved through a fluid produces an aerodynamic force. The component of this force perpendicular to the direction of motion is called lift while the component parallel to the direction of motion is called drag (Gad-el-Hak, 2000). The lift on an airfoil is primarily the result of its angle of attack and shape. When oriented at a suitable angle, the airfoil deflects the oncoming air, resulting in a force on the airfoil in the direction opposite to the deflection. This force is known as aerodynamic force and can be resolved into two components: Lift and drag. Most airfoil shapes require a positive angle of attack to generate lift, but cambered airfoils can generate lift at zero angle of attack. National Advisory committee for Aeronautics (NACA) four and five digit designs have been used for early modern wind turbines (Schubel and Crossley, 2012). The classification shows the geometric profile of a NACA aerofoil where the 1st digit refers to maximum chamber to chord ratio, 2nd digit is the camber position in tenths of the chord and the 3rd and 4th digits are the maximum thickness to chord ratio in percent.(Schubel and Crossley, 2012). The use of a single aerofoil for the entire blade length would results in inefficient design (Maalawi and Badr, 2003). Each section of the blade has a differing relative air velocity and structural requirement and therefore should have its aerofoil section tailored accordingly .at the root, the blade sections have large maximum thickness which is essential for the intensive loads carried resulting in thick profiles. Approaching the tip blades blend into thinner sections with reduced load, higher linear velocity and increasingly critical aerodynamic performance. From some selected review of literature;

Saxena and kumar (2015) performs wind tunnel experiment to find out the aerodynamic characteristics of NACA4412 Airfoil and NREL S809 airfoil. Eleni et al., (2012), Patel et al., 2014) presented a two dimensional subsonic flow over NACA0012 airfoil at various angles of attack with spalart-Allmaras turbulence models using computational fluid dynamics. Result shows that the model used does not give accurate results at high angles of attack.

Kumar et al., (2016) carried out CFD analysis to compare the aerodynamic characteristics of NACA4412 Airfoil and NREL S809 airfoil. Result shows that NACA4412 airfoil exhibits better aerodynamics performance for all range of angle of attacks than NREL S809 airfoil.
Rao and sampath (2014) carried out a conceptual study of performance enhancing devices for NACA4412 airfoil using computational fluid dynamics. Their aim was to improve airfoil performance at high angle-of-attack. Saraf et al., (2017) analyzed a two dimensional NACA0012 airfoil using computational fluid dynamics software. Ravi et al., (2013) investigated numerical aerodynamic phenomena in the post-stall region using computational fluid dynamics with spalart allmaras-turbulence model. Simo et al., (2007) presented a systematic analysis of a single-bladed 2D VAWT configuration with NACA0015 airfoil using CFD comparing with particle image velocimetry (PIV). The comparison shows the non-suitability of one equation turbulence model for the highly unsteady problem. In this present study, an attempt was made to investigate the performance of some selected airfoil for the production of wind turbine blade using Computational Fluid Dynamics.

2. Methodology of Research

The step by step methodology employed for this study is described as follows;

2.1 Geometry Creation

The various airfoils geometry were created using Autodesk inventor and imported into ANSYS design modeler. The profiles were generated using the information presented in Table 1 while the resulting 2D Airfoil generated from the ANSYS design modeller is shown in Figures 1, 2 and 3 respectively.

Table 1 Airfoil: design data

	NACA 0012	NACA 2412	NACA 4412
Maximum Camber (0-9)	0	2	4
Maximum Camber Position (0-9)	0	4	4
Thickness (0-99)	12	12	12
Chord length	1m	1m	1m

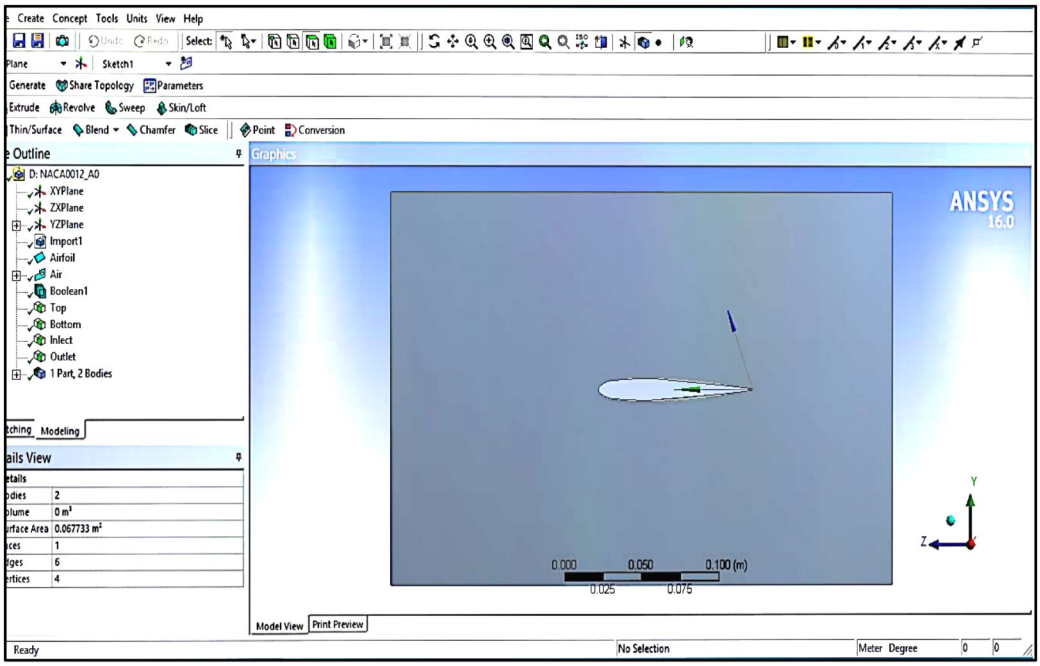

Figure 1: NACA0012 geometry

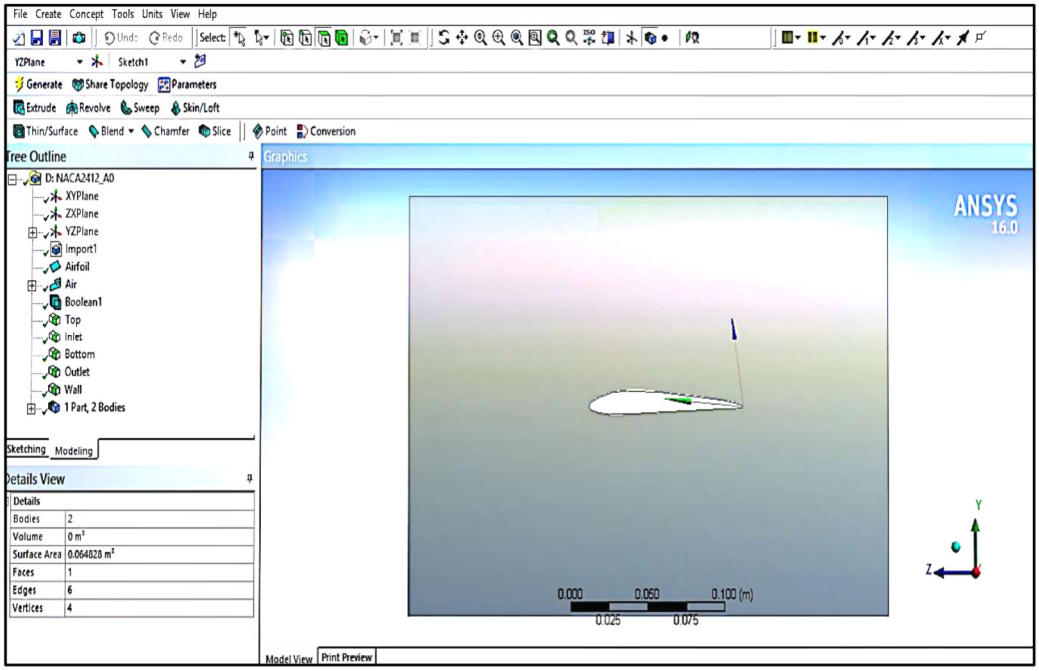

Figure 2: NACA2412 geometry

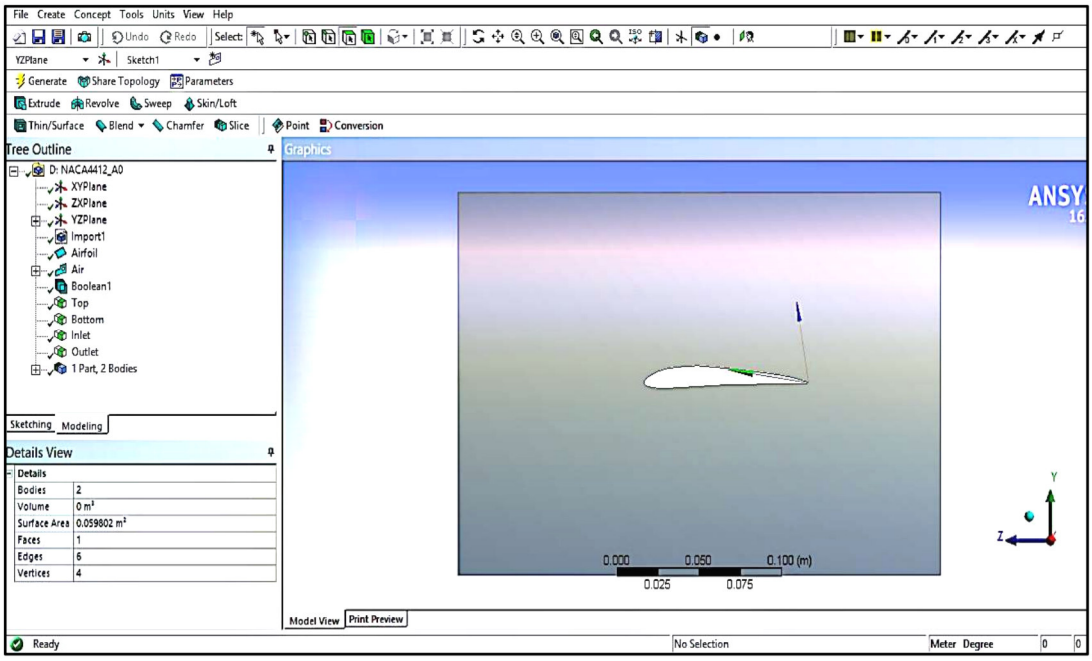

Figure 3: NACA4412 geometry

2.2: Mesh generation

To mesh the airfoil fluid geometry, ANSYS Meshing was used. In the meshing application, the following settings were used; Physics preference: CFD, Units: Metric (m, kg, N, s, V, A) while the fluid part is automatically transferred to ANSYS Meshing application. The mesh method was set at automatic (Patch conforming/sweeping mode) and the boundaries of the fluid body was named by creating named selections at the edges of the fluid body. This is done to enable easy application of boundary conditions in FLUENT. The Mesh was subsequently generated by clicking the Update button. The preview of the mesh is shown in Figure 4

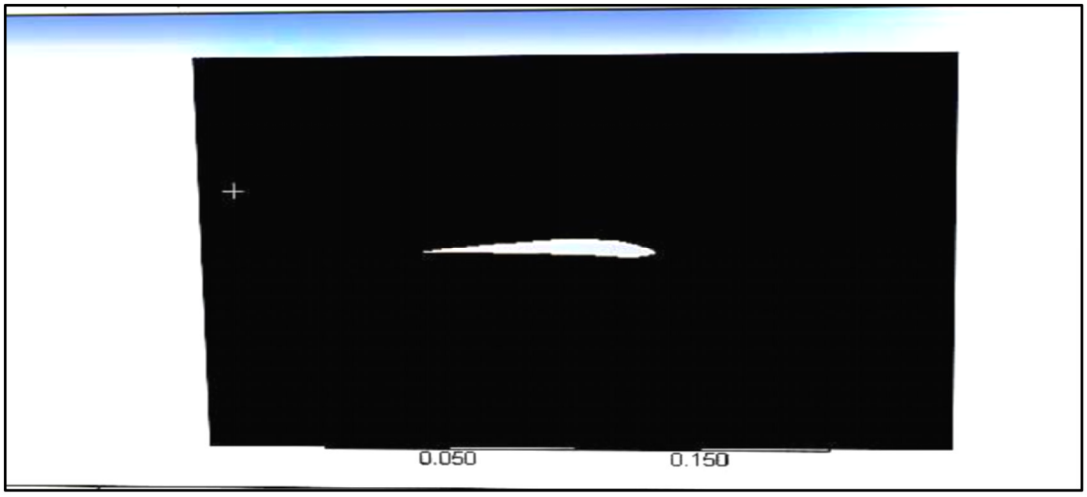

Figure 5: Preview of generated Mesh

The mesh total nodes were observed to be 12405 with total elements of 24810. The Mesh files of the airfoil fluid part are automatically transferred to the setup cell.

2.3: Problem Setup

On completion of the meshing step, ANSYS FLUENT two dimensional analysis module was subsequently launched. For the two dimensional analysis modules, the pressure based solver is selected by default while the spalart-Allmaras turbulence model was checked for adoption. Air with density of 1.225 Kg/m^3, viscosity of 1.780E-04 Kg/m-s and operating pressure of 101325Pa was selected as the fluid material for the fluid volume.

2.4: Boundary Conditions

The following boundary conditions presented in Table 2 were adopted for this study

Table 2: Selected boundary conditions for ANSYS implementation

S/N	Boundary Elements	Conditions
1	Zone: Airfoil	Boundary Type: Wall
2	Zone: Inlet	i. Boundary Type: Velocity Inlet ii. Velocity Specification Method: Magnitude, Normal to Boundary iii. Velocity Magnitude: 14.87m/s, Turbulent viscosity ratio: 10
3	Zone: Outlet	Gauge Pressure: 0 Pa

2.5: Monitors

The residuals for X velocity, Y velocity, Turbulence and Continuity were all set at 1e-07. The residual for. Lift and Drag monitors were also plotted and printed to screen during the simulation for the Airfoil wall zone only. The X and Y values ensure that the drag coefficient is calculated parallel to the free stream flow which is 4˚ off the global coordinates.

2.6: Solution Initialization

The solution was initialized using the Hybrid Initialization method. Hybrid Initialization is most applicable for flows in complex topologies because it provides better initial velocity and pressure fields than the standard initialization and helps in improving the convergence behavior of the solver.

3. Results and Discussion

Results of Table 3 shows the lift coefficients, Drag coefficients, lift, drag and lift/drag ratio of the various airfoils and angle of attack considered.

Table 3: Simulated Lift and Drag for the various Airfoils

S/N	Airfoil Name	Angle of Attack	Lift Coefficient	Draft Coefficient	Lift	Drag	Lift/Drag Ratio
1	NACA0012	0°	2.0816e-02	1.32	2.8192	178.773	0.01577
2	NACA0012	4°	1	1.775	135.434	240.395	0.56338
3	NACA0012	8°	1.768	2.726	239.447	369.193	0.64857
4	NACA0012	12°	1.98	4.07	268.159	551.216	0.48649
5	NACA2412	0°	0.724	1.321	98.054	178.91	0.54806
6	NACA2412	4°	1.35	1.465	182.836	198.411	0.92150
7	NACA2412	8°	1.82	2.026	246.49	274.389	0.89832
8	NACA2412	12°	2.75	2.975	372.444	402.916	0.92437
9	NACA4412	0°	1.08	1.285	146.269	174.033	0.84047
10	NACA4412	4°	4.75	1.7150	643.312	232.269	2.76969
11	NACA4412	8°	4.02	2.2	544.444	297.9548	1.82727
12	NACA4412	12°	4.85	3.725	612.974	423.231	1.55200

From the result of Table 3, it was observed that NACA4412 at 4^0 angle of attack; gave the highest lift to drag ratio. Figures 5 to 10 show the static pressure and velocity magnitude of the various airfoils and the corresponding angle of attack.

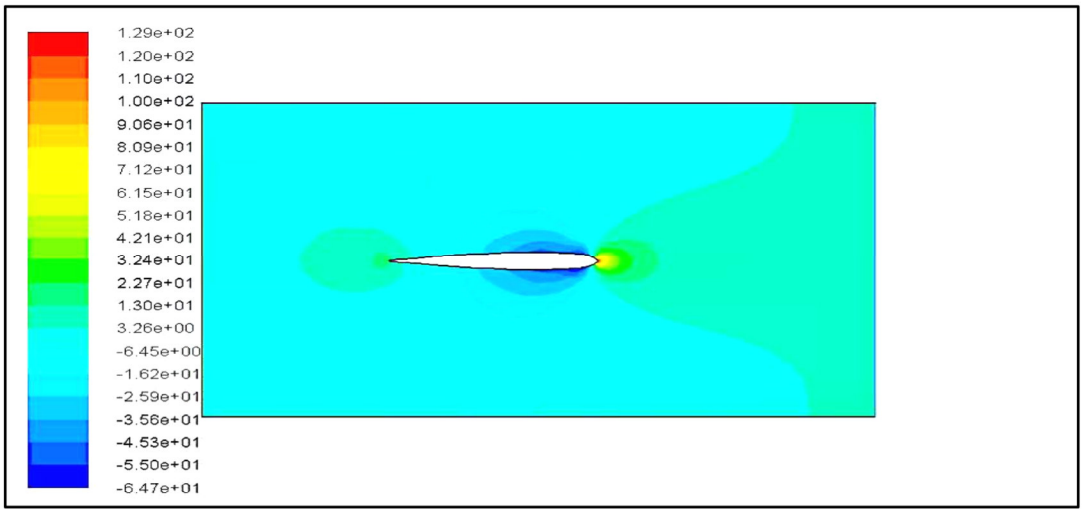

Figure 5: Contour of static pressure for NACA 0012 at 0° angle of attack

For an angle of attack of 0 degree, the contours of static pressure over an airfoil is symmetrical for above and lower sections and the stagnation point is exactly at the nose of an aerofoil. Hence, there are no pressure difference created between the two faces of aerofoil at **0°** angle of attack.

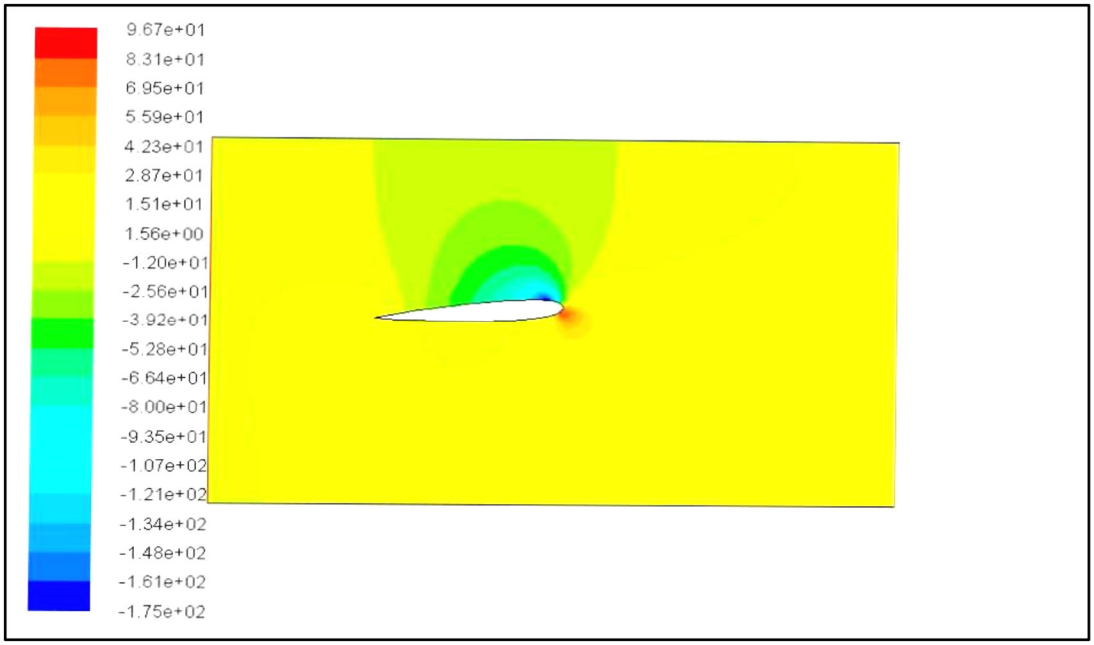

Figure 6: Contour of static pressure for NACA 0012 at 4° angle of attack

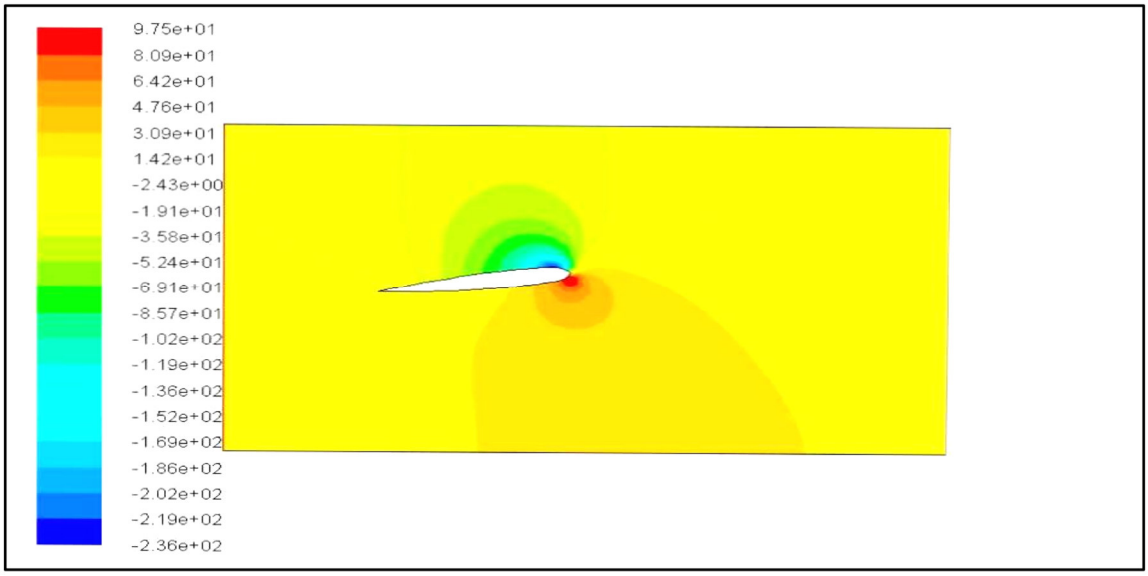

Figure 7: Contour of static pressure for NACA 0012 at 8° angle of attack

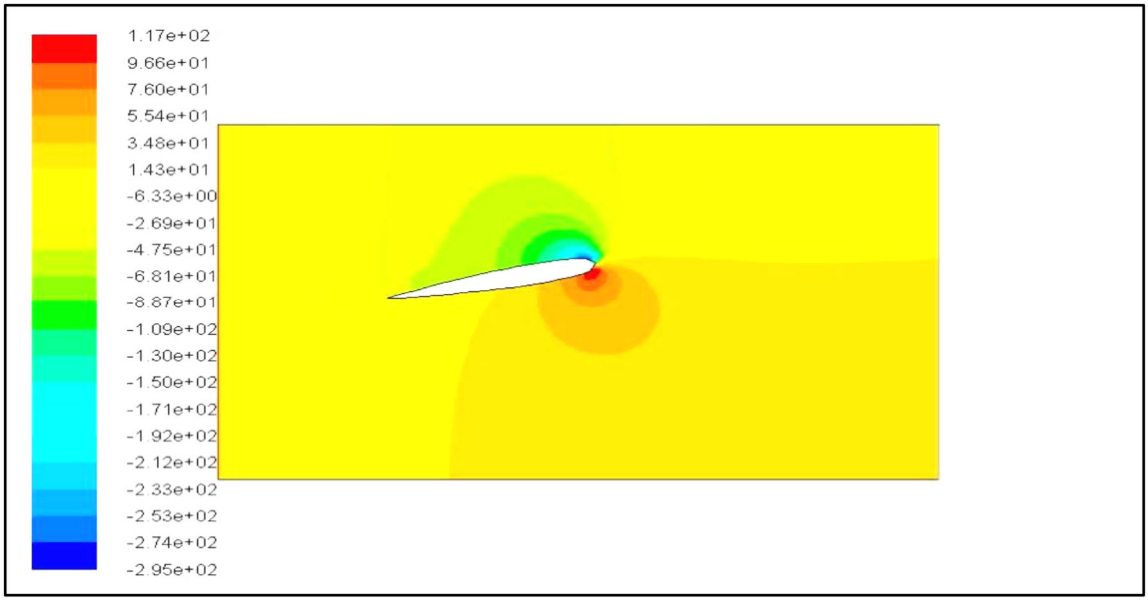

Figure 8: Contour of static pressure for NACA 0012 at 12° angle of attack

Figures 6.7,8 present the contour of static pressure for NACA 0012 and 4°, 8°, 12°, angle of attack is. For an angle of attack of 4 degree, 8 degree, 12 degree, the flow has a stagnation point just under the leading edge and hence producing lift as there is a low pressure region on the upper surface of the foil. It can also be observed that Bernoulli's principle is holding true; the velocity is high (denoted by the red contours) at the low pressure region and vice-versa. There is a region of high pressure at the leading edge (stagnation point) and region of low pressure on the upper surface of airfoil.

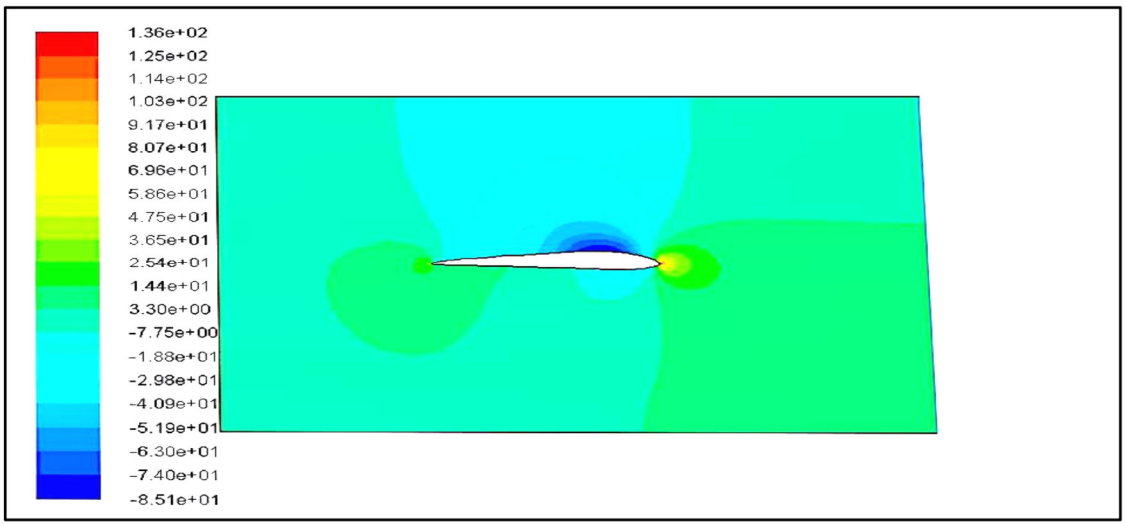

Figure 9: Contour of static pressure for NACA 2412 and 0° angle of attack

The contour of static pressure for NACA 2412 and 0° angle of attack is presented in Figure 9. For an angle of attack of 0 degree, the contours of static pressure over an airfoil is symmetrical for above and lower sections and the stagnation point is exactly at the nose of an aerofoil. Hence, there are no pressure different created between two faces of aerofoil at zero degree of an angle of attack.

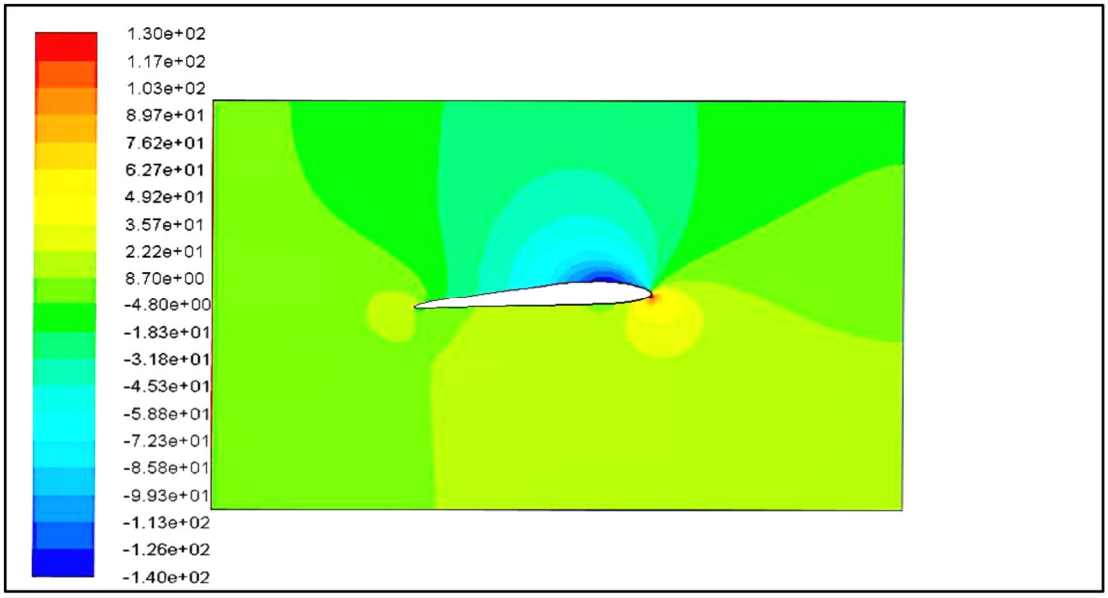

Figure 10: Contour of static pressure for NACA 2412 and 4° angle of attack

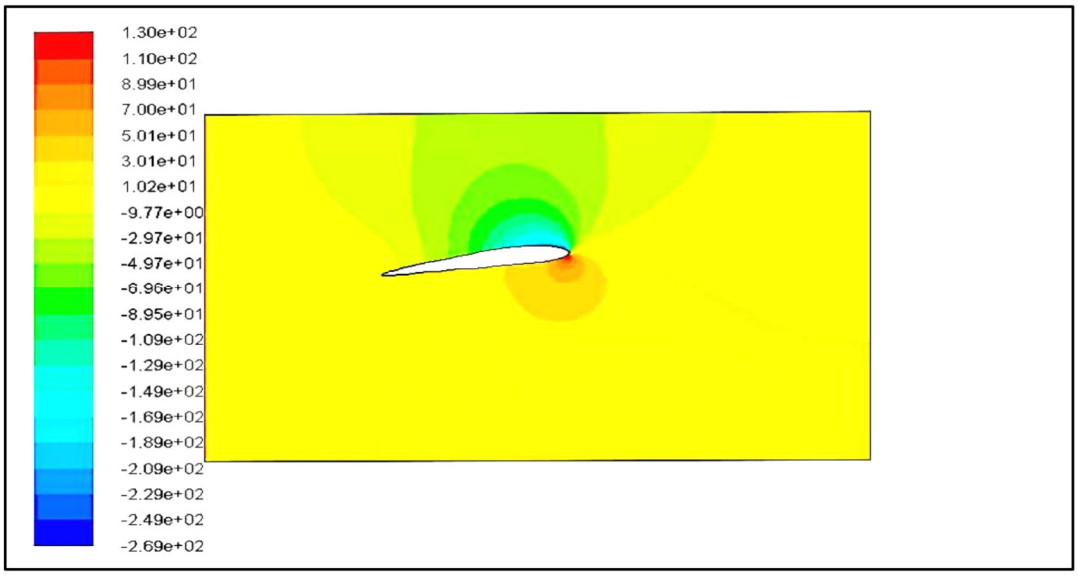

Figure 11: Contour of static pressure for NACA 2412 and 8° angle of attack

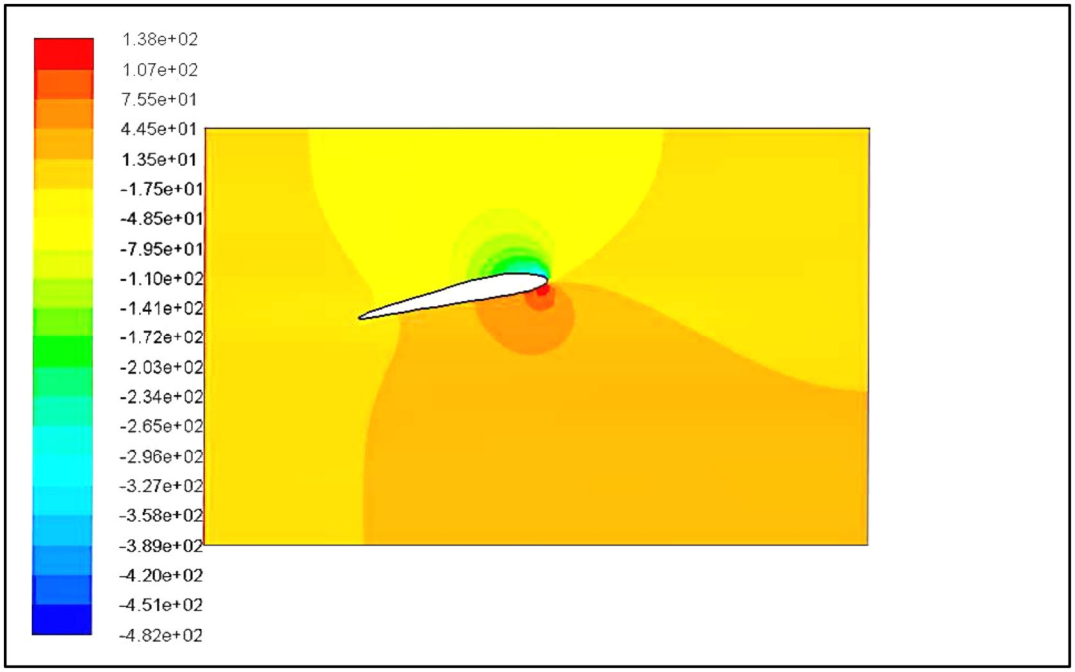

Figure 12: Contour of static pressure for NACA 2412 and 12° angle of attack

Figures 10, 11 and 12 present the contour of static pressure for NACA 2412 and 4°, 8° 12°, angle of attacks. For an angle of attack of 12 the flow has a stagnation point just under the leading edge and hence producing lift as there is a low pressure region on the upper surface of the foil. It can also be observed that Bernoulli's principle is holding true; the velocity is high (denoted by the red contours) at the low pressure region and vice-versa. There is a region of high pressure at the leading edge (stagnation point) and region of low pressure on the upper surface of airfoil.

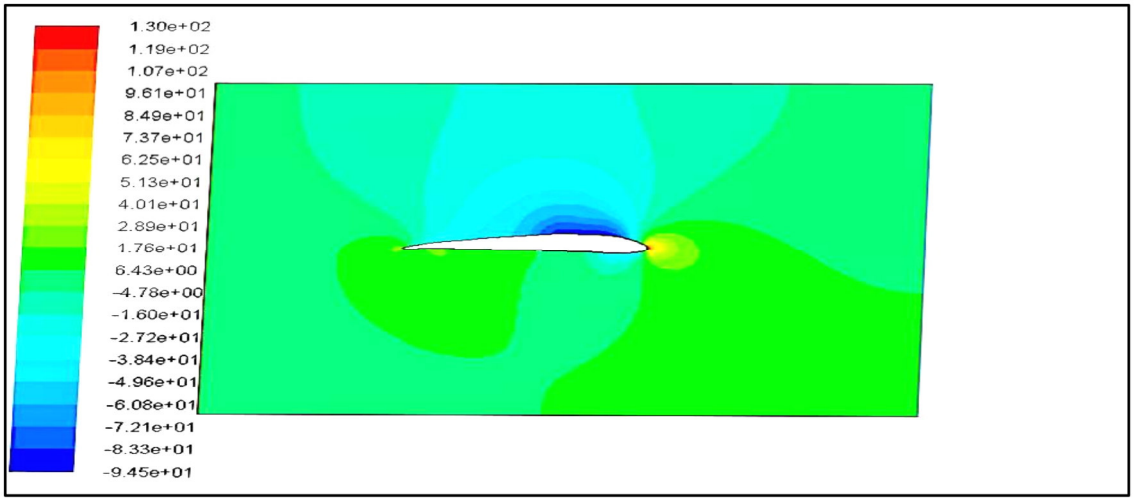

Figure 13: Contour of static pressure for NACA 4412 and 0° angle of attack

The contour of static pressure for NACA 4412 and 0° angle of attack is presented in Figure 13. For an angle of attack of 0 degree, the contours of static pressure over an airfoil is symmetrical for above and lower sections and the stagnation point is exactly at the nose of an aerofoil. Hence, there are no pressure different created between two faces of aerofoil at zero degree of an angle of attack.

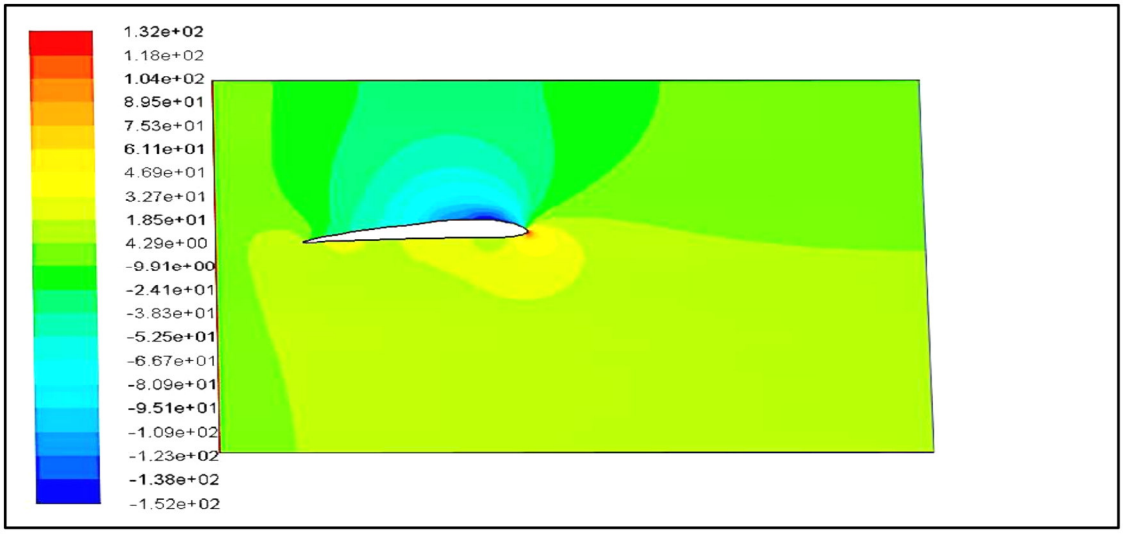

Figure 14: Contour of static pressure for NACA 4412 and 4° angle of attack

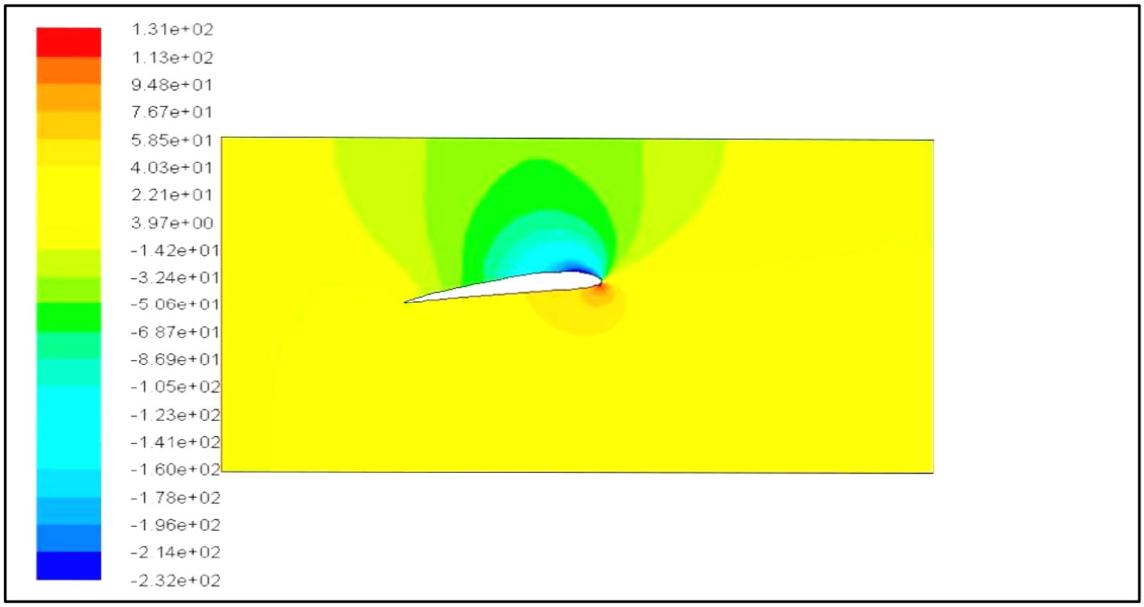

Figure 15: Contour of static pressure for NACA 4412 and 8° angle of attack

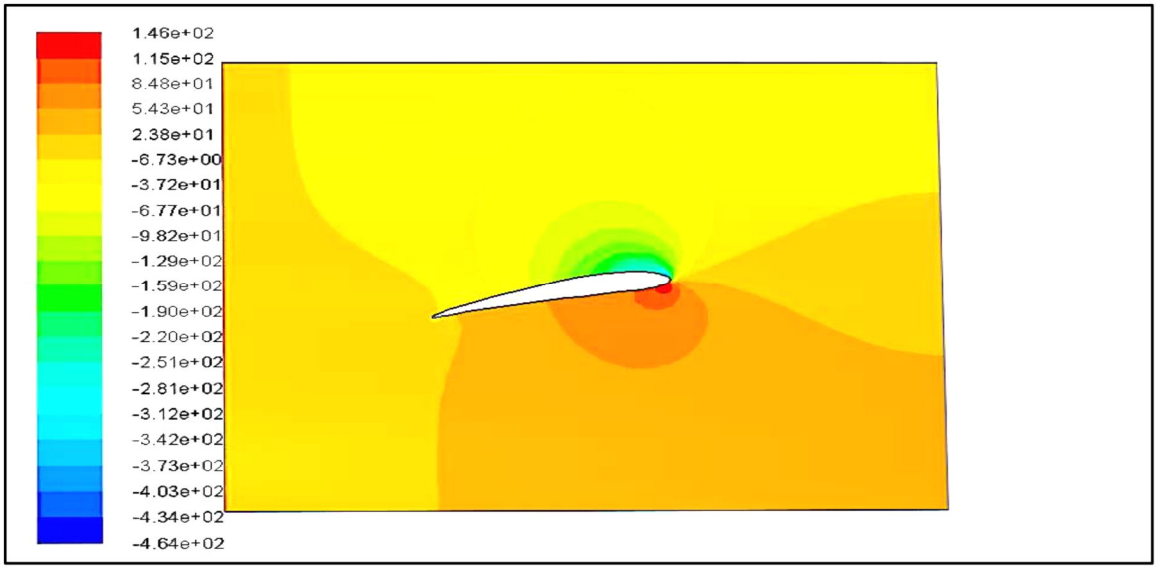

Figure 16: Contour of static pressure for NACA 4412 and 12° angle of attack

Figures 14,15 and 16 presents the contour of static pressure for NACA 4412 and 4° angle of attack are depicted below. For an angle of attack of 4 degree, the flow has a stagnation point just under the leading edge and hence producing lift as there is a low pressure region on the upper surface of the foil. It can also be observed that Bernoulli's principle is holding true; the velocity is high (denoted by the red contours) at the low pressure region and vice-versa. There is a region of high pressure at the leading edge (stagnation point) and region of low pressure on the upper surface of airfoil

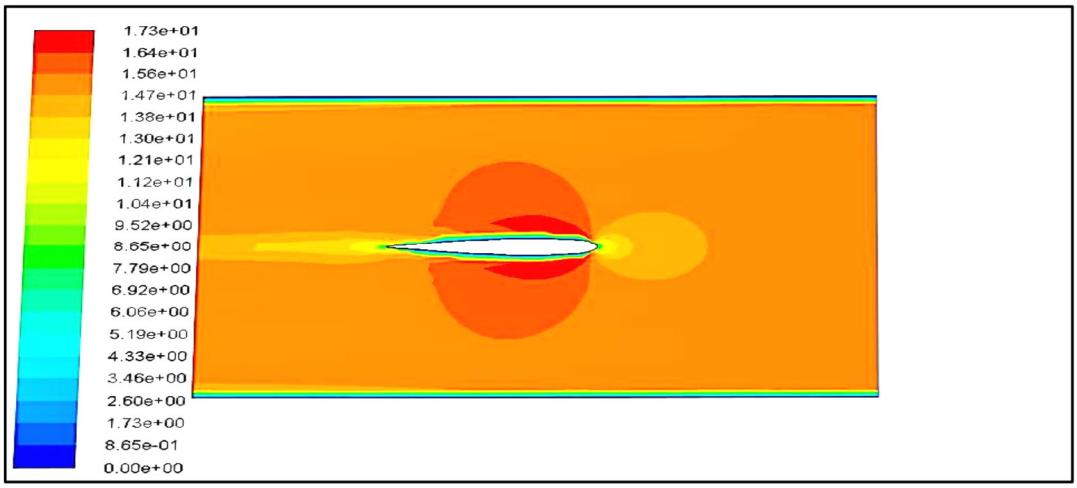

Figure 17: Contour of velocity magnitude for NACA 0012 and 0° angle of attack

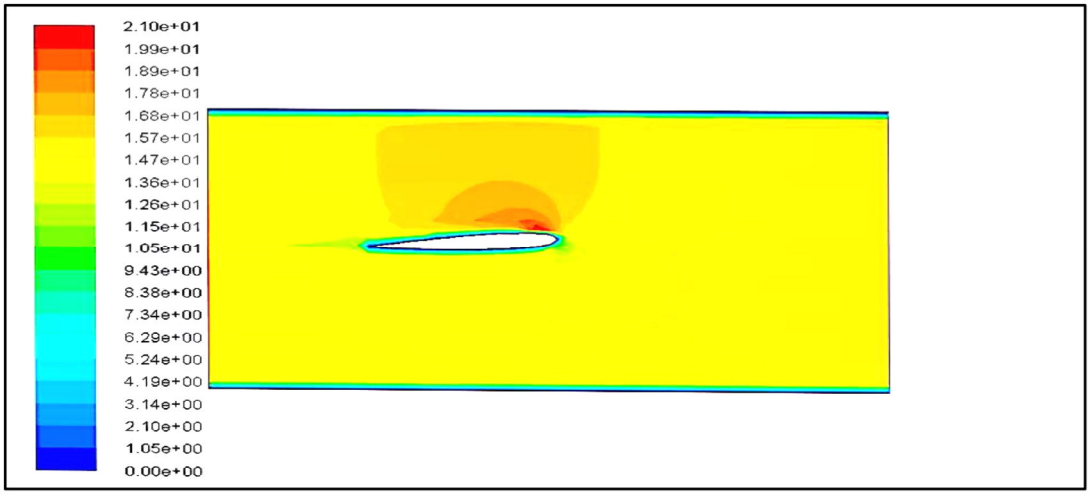

Figure 18: Contour of velocity magnitude for NACA 0012 and 4° angle of attack

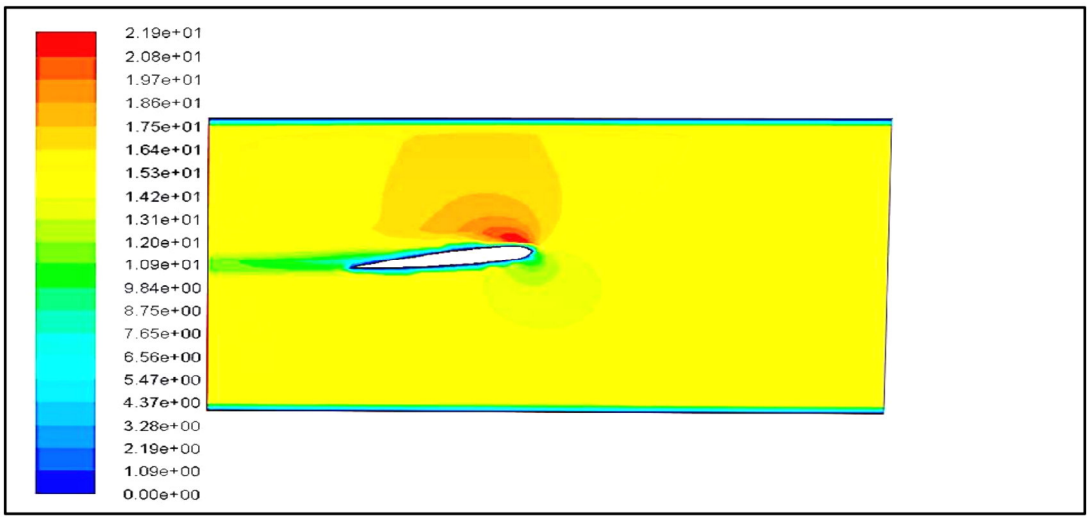

Figure 19: Contour of velocity magnitude for NACA 0012 and 8° angle of attack

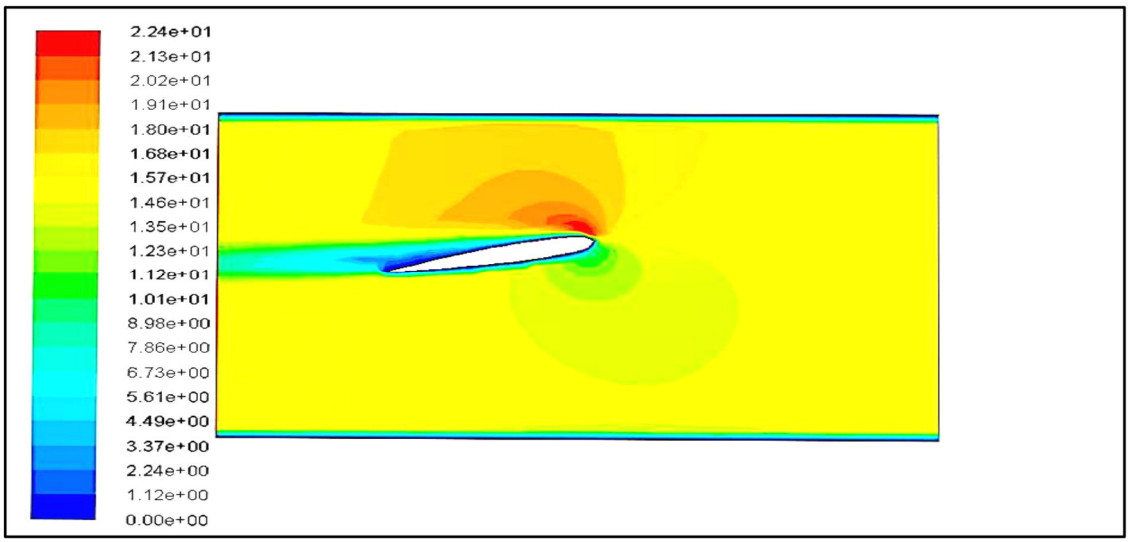

Figure 20: Contour of velocity magnitude for NACA 0012 and 12° angle of attack

The contour of velocity magnitude for NACA 0012 at 0^0, 4^0, 8^0 and 12^0 angle of attack is presented in Figures 17, 18, 19 and 20 respectively. For an angle of attack of 0^0, the contours of velocity magnitude for

NACA 0012 are same and symmetrical. At 4^0, 8^0 and 12^0, angles of attack the stagnation point is slightly shifted towards the trailing edge via bottom surface hence it will create low velocity region at lower side of the NACA airfoil and higher velocity acceleration region at the upper side of the airfoil. According to Bernoulli's principle upper surface will gain low pressure and lower surface will gain higher pressure. Hence, value of lift coefficient will increase and drag coefficient will also increase; but the increase in drag is low compare to increase in lift force. In a symmetrical NACA airfoil at no incidence, the distribution of velocity and thus the pressures along both surfaces would have been exactly the same, canceling each other to a resulting total lift force of zero.

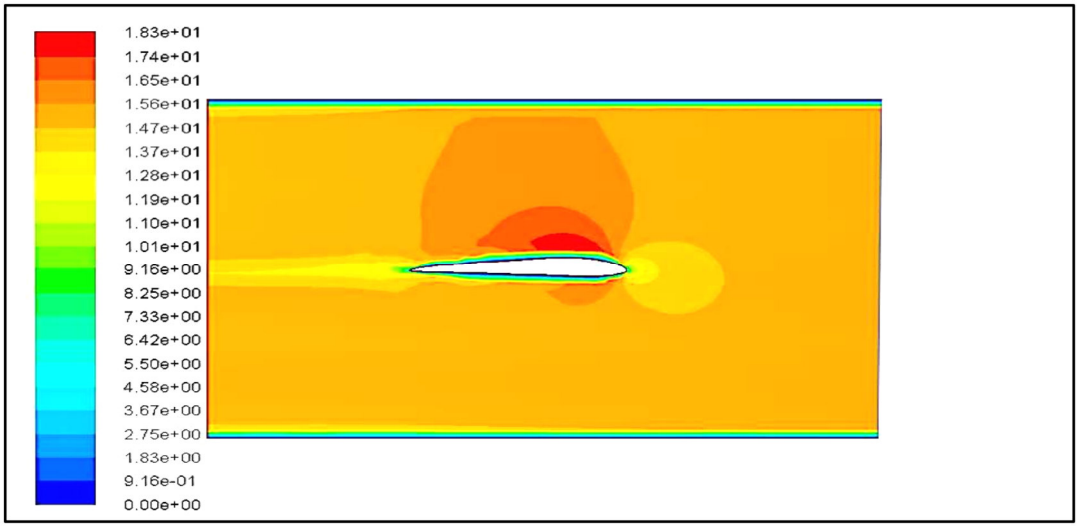

Figure 21: Contour of velocity magnitude for NACA 2412 and 0° angle of attack

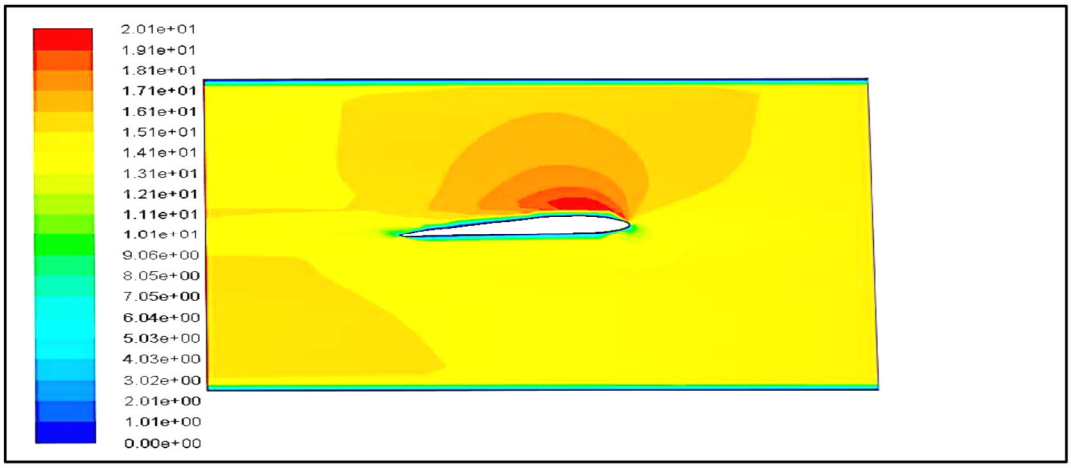

Figure 22: Contour of velocity magnitude for NACA 2412 and 4° angle of attack

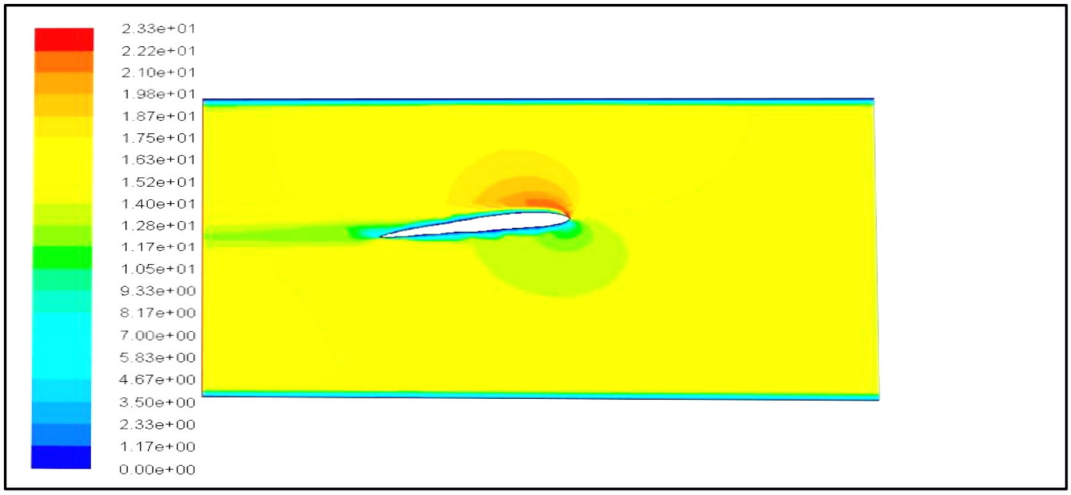

Figure 23: Contour of velocity magnitude for NACA 2412 and 8° angle of attack

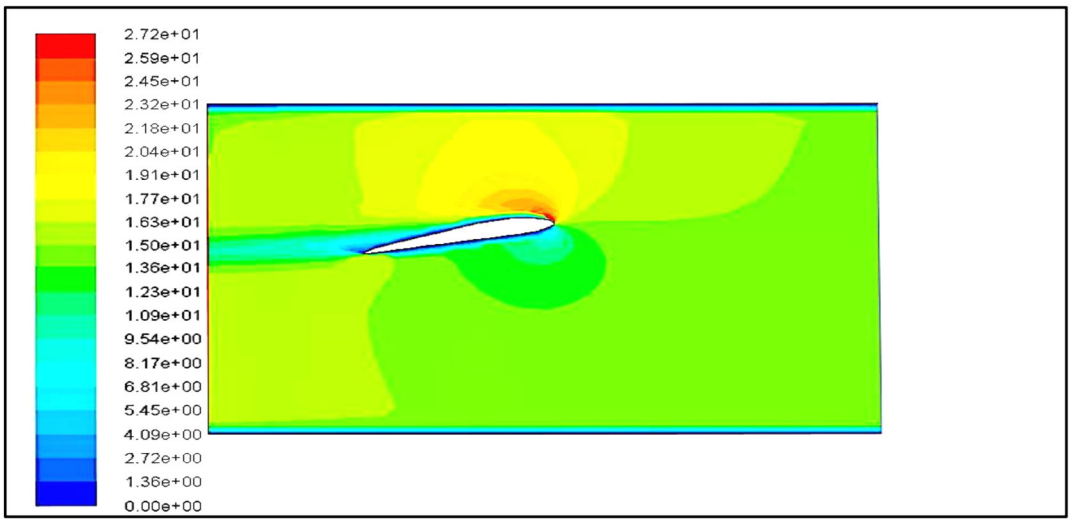

Figure 24: Contour of velocity magnitude for NACA 2412 and 12° angle of attack

The Contour of velocity magnitude for NACA 2412 and 0^0, 4^0, 8^0 and 12^0, angles of attack is presented in Figures 21, 22, 23 and 24 respectively. For an angle of attack of 0^0, the contours of velocity magnitude for NACA 2412 are same and symmetrical. At 4^0, 8^0 and 12^0, angles of attack, the stagnation point is slightly shifted towards the trailing edge via bottom surface hence it will create low velocity region at lower side of the NACA airfoil and higher velocity acceleration region at the upper side of the airfoil and according to Bernoulli's principle upper surface will gain low pressure and lower surface will gain higher pressure. Hence value of lift coefficient will increase and drag coefficient will also increase but the increasing in drag is low compare to increasing in lift force. In a symmetrical NACA airfoil at no incidence, the distribution of velocity and thus the pressures along both surfaces would have been exactly the same, canceling each other to a resulting total lift force of zero.

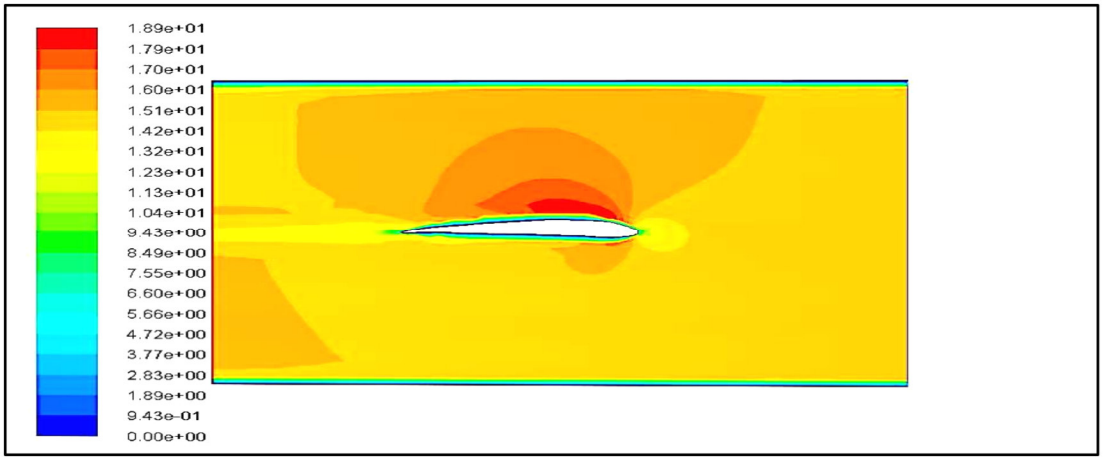

Figure 25: Contour of velocity magnitude for NACA 4412 and 0° angle of attack

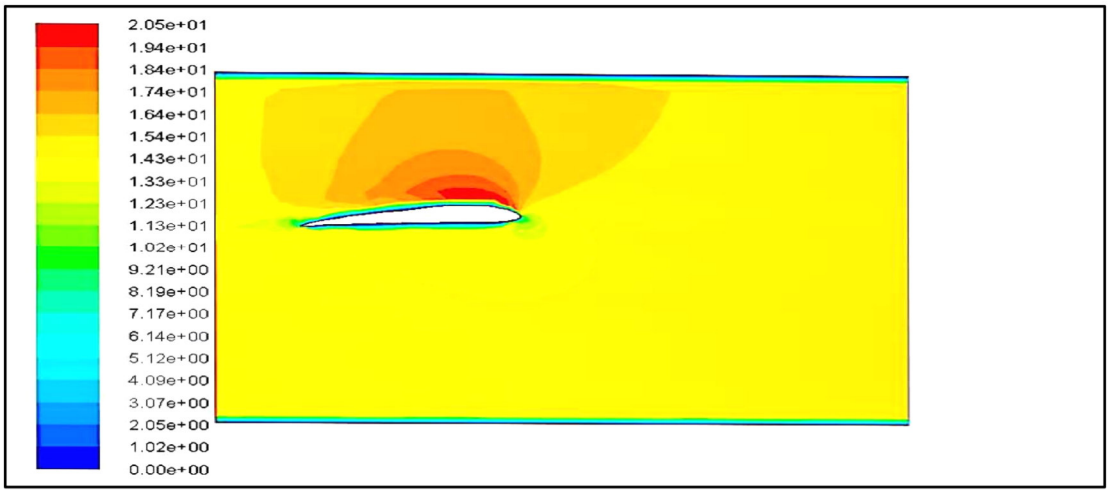

Figure 26: Contour of velocity magnitude for NACA 4412 and 4° angle of attack

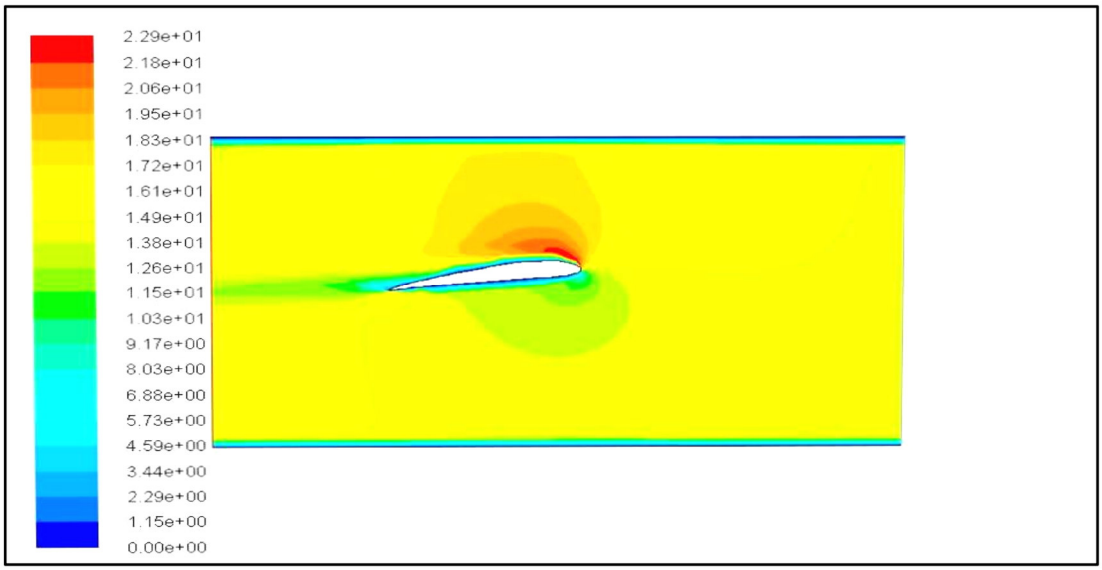

Figure 27: Contour of velocity magnitude for NACA 4412 and 8° angle of attack

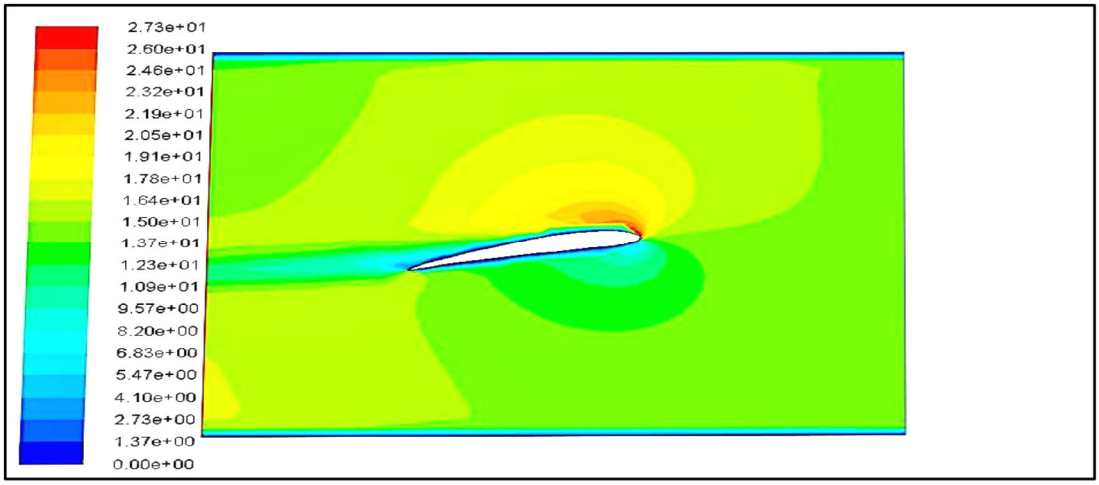

Figure 28: Contour of velocity magnitude for NACA 4412 and 12° angle of attack

The Contour of velocity magnitude for NACA 4412 and 0^0, 4^0, 8^0 and 12^0 angles of attacks are presented in Figures 25, 26, 27 and 28 respectively. For an angle of attack of 0^0, the contour of velocity magnitude for NACA 4412 are same and symmetrical and at 4^0, 8^0 and 12^0 angles of attacks the stagnation point is slightly shifted towards the trailing edge via bottom surface hence it will create low velocity region at lower side of the NACA airfoil and higher velocity acceleration region at the upper side of the airfoil and according to Bernoulli's principle upper surface will gain low pressure and lower surface will gain higher pressure. Hence value of lift coefficient will increase and drag coefficient will also increase but the increasing in drag is low compare to increasing in lift force. In a symmetrical NACA airfoil at no incidence, the distribution of velocity and thus the pressures along both surfaces would have been exactly the same, canceling each other to a resulting total lift force of zero.

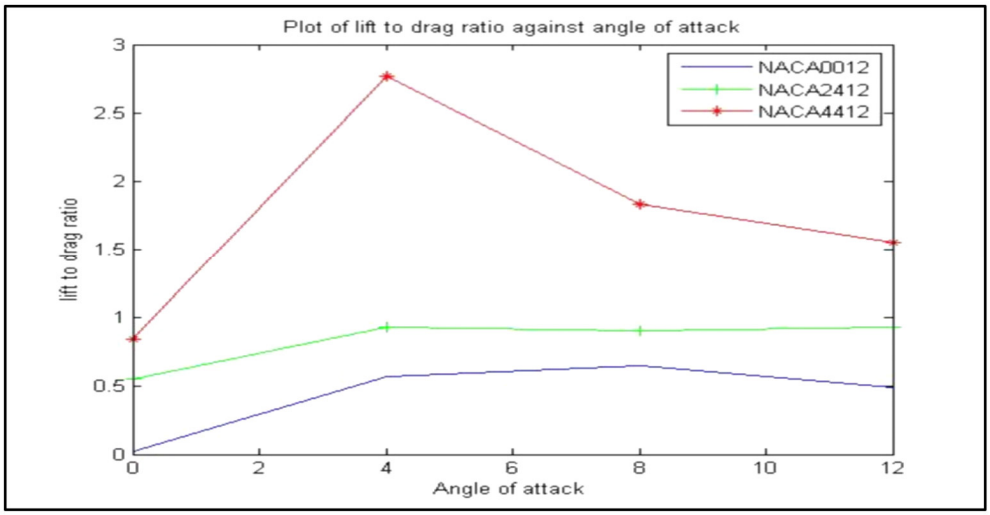

Figure 29: Plot of lift to drag ratio against angle of attack

Figure 29 shows the plot of lift to drag ratio of NACA0012, NACA2412 and NACA4412 at 0^0, 4^0, 8^0 and 12^0 angles of attack. It is obvious from the plot of Figure 29 that NACA4412 at 4^0 angle of attack gave the highest lift to drag ratio of 2.76969 and hence consider for wind turbine blade design.

4. Conclusion

A CFD study on the various NACA Airfoil designs at different angle of attack was carried out in order to determine the best configuration that will be most suitable for the wind turbine blade in this environment. The simulation was carried out on NACA 0012, NACA 2412 and NAC 4412 Airfoils varying their angle of attack from 0°, 4°, 8° and 12° using ANSYS Fluent version 16.0. The contour plot of the static pressure and velocity magnitude obtained are consistent with results presented in literatures. Increase in lift has a positive impact on power produced by the blade as well as the lift to drag ratio. Also the resultant velocity increased with increase of the angle of attack. From the plots presented above, it can be observed that NACA 4412 at 4° angle of attack gave the maximum lift to drag ratio and hence is considered to be most suitable for the design of the blade.

5. References

Eleni, C.D; Dionissios, P and Tsavalos, I. A. (2012), Evaluation of the turbulence models for the simulation of the flow over NACA4412 airfoil, *Journal of Mechanical Engineering Research,* Vol. 4(3), pp. 100-111.

Eriksson, S, Bernhoff, H and Leijon, M (2006), Evaluation of different turbine concepts for wind power, Renewable and Sustainable Energy Reviews 1224 Science Direct. Web. 9 Dec. 2011.

Fuglsang, P, Bak, C (2004), Development of the RISO wind turbine airfoils, wind Energy, vol.7, pp.145-162.

Gad-el-Hak (2000), Flow Control Passive: Active and Reactive Flow Management, First ed., Cambridge University Press, 2000.

Kaminsky, C; Filush, A; Kasprzak, P and Mokhtar, W (2011) A CFD Study of Wind Turbine Aerodynamics', Proceedings of the ASEE North Central Section Conference Copyright © 2012, American Society for Engineering Education

Kumar, B.N, Paramasivam, K.M, Prasanna, M and Karis, A.Z.G.M (2016), computational fluid dynamics analysis of aerodynamic characteristics of NACA4412 VS S809 Airfoil for wind turbine applications, international journal of advanced engineering technology, vol.7, no.3, pp.168-173

Maalawi, K.Y and Badr, M.A (2003), A Practical approach for selecting optimum wind rotors, Renew. Energy, Vol.28, PP.803 – 822

Patel, K.S, Patel, S.B, Patel, U.B and Ahuja, A (2014), CFD analysis of an aerofoil, international journal of engineering research, vol.3, no.3, pp.154-158

Ravi, H.C, Madhukeshwara, N and Kumarappa, S (2013), Numerical investigation of flow transition for NACA4412 Airfoil using computational fluid dynamics, international Journal of innovative research in science, Engineering and Technology, vol.2, no.7, pp.2778-278

Rooij, R.P.J.O.M. Timmer, W (2003), Roughness sensitivity considerations for thick rotor blade airfoils, J. Solar Energy, Eng. Trans. ASME, Vol,125,pp.468-478

Saraf, A.KM Singh, M.P and Chouhan, T.S (2017), Aerodynamic analysis of NACA0012 Airfoil using CFD, international Journal of mechanical and production engineering, vol.5, no.12. pp: 21-25

Saxena, S and Kumar, R (2015), design of NACA2412 and its analysis at different angle of attacks, Reynolds numbers, and a wind tunnel test, international journal of engineering research and general science, vol.3, no.2. pp: 193-200

Schubel, P.J and Crossley, R.J (2012), Wind Turbine Blade Design, Energies, Vol.5, PP.3425-3449

Simao-Ferreira, C. J., Van-Brussel, G. J. W., and Van-Kuik, G., 2d CFD Simulation of Dynamic Stall on a Vertical Axis Wind Turbine: Verification and Validation with PIV Measurements, *45th AIAA Aerospace Sciences Meeting and Exhibit*, Reno, Nevada, 2007.